JOURNAL OF VIROLOGY, Mar. 2011, p. 2953–2963 Vol. 85, No. 6
0022-538X/11/$12.00 doi:10.1128/JVI.02020-10

Subcellular Localization and Rearrangement of Endoplasmic Reticulum by Brome Mosaic Virus Capsid Protein▽

Devinka Bamunusinghe, Jang-Kyun Seo, and A. L. N. Rao*

Department of Plant Pathology and Microbiology, University of California, Riverside, California 92521-0122

Received 22 September 2010/Accepted 29 December 2010

Genome packaging in the plant-infecting *Brome mosaic virus* (BMV), a member of the alphavirus-like superfamily, as well as in other positive-strand RNA viruses pathogenic to humans (e.g., poliovirus) and animals (e.g., *Flock House virus*), is functionally coupled to replication. Although the subcellular localization site of BMV replication has been identified, that of the capsid protein (CP) has remained elusive. In this study, the application of immunofluorescence confocal microscopy to *Nicotiana benthamiana* leaves expressing replication-derived BMV CP as a green fluorescent protein (GFP) fusion, in conjunction with antibodies to the CP and double-stranded RNA, a presumed marker of RNA replication, revealed that the subcellular localization sites of replication and CP overlap. Our temporal analysis by transmission electron microscopy of ultrastructural modifications induced in BMV-infected *N. benthamiana* leaves revealed a reticulovesicular network of modified endoplasmic reticulum (ER) incorporating large assemblies of vesicles derived from ER accumulated in the cytoplasm during BMV infection. Additionally, for the first time, we have found by ectopic expression experiments that BMV CP itself has the intrinsic property of modifying ER to induce vesicles similar to those present in BMV infections. The significance of CP-induced vesicles in relation to CP-organized viral functions that are linked to replication-coupled packaging is discussed.

Positive-strand RNA viruses cause serious diseases in humans, animals, and plants. The onset of a viral disease and its progression relies on coordinated strategies of the host cell infrastructure and metabolism. Nonenveloped and enveloped viruses with positive-stranded RNA genomes induce a variety of membrane alterations with several morphologies that house replication complexes (22, 29). Some commonly found intracellular membrane alterations include spherule invaginations (e.g., *Flock House virus* [FHV] and *Brome mosaic virus* [BMV]), rosettes (e.g., poliovirus), double-membrane vesicles (DMV), and convoluted membranes (e.g., severe acute respiratory syndrome [SARS] and dengue viruses) (29). Although the endoplasmic reticulum (ER) appears to be the preferred cellular membrane site for the replication of poliovirus (40), SARS (44), dengue virus (54), potyviruses (22, 39, 53), and BMV (38), other cellular organelles, such as mitochondria (FHV) (28), lysosomes (rubella and *Semliki Forest virus*) (21) peroxisomes, and chloroplasts (*Tomato bushy stunt virus*) (7, 22) are also used as sites for RNA replication. To date, only nonstructural proteins, mostly viral replicase proteins, have been implicated in the induction of these membrane alterations seen in virus-infected cells (13, 25).

BMV is the type species of the genus *Bromovirus* (18, 33). It belongs to the *Bromoviridae* family of plant viruses and is a representative member of the alphavirus-like super family of positive-strand RNA viruses (18). BMV has been an ideal model system for uncovering many aspects of eukaryotic RNA virus replication (30) and assembly (34). The genome of BMV is divided among three RNA components. Viral replication is dependent on two nonstructural proteins, 1a (containing both an RNA-helicase-like domain and a capping domain) and 2a (containing a polymerase domain), encoded, respectively, by genomic RNA1 and -2 (1). Genomic RNA3 is dicistronic and dispensable for replication (33). The 5′ open reading frame (ORF) of RNA3 encodes a nonstructural 3a movement protein (MP) required for cell-to-cell movement, while the capsid protein (CP) encoded in the 3′ half is expressed via a subgenomic RNA (sgRNA4) produced during replication (33). Replication of BMV has been studied in detail at the molecular and subcellular level using plant protoplasts (37) and a surrogate yeast system (37, 43). Early in BMV replication, an interaction between 1a and reticulon homology proteins (RHP) results in the induction of negatively curved ER-derived spherule-like invaginations (14). Then, 2a interacts with 1a (11) and recruits viral RNAs to these spherules to initiate replication (42).

Plant viral CP is multifunctional (9). Two important phases in the BMV life cycle implicate the existence of an intimate relationship between CP and replication. First, CP is involved in the upregulation of plus-strand synthesis over minus strands (9, 26). Second, CP translated from a replication-derived mRNA exclusively encapsidates the progeny RNA into stable infectious virions (3, 4), a process commonly referred to as replication-coupled packaging that is highly conserved among many positive-strand RNA viruses (3, 19, 31, 48). Although the subcellular localization site of BMV replication has been delineated to ER-derived spherules (38, 42), that of the CP is not known. Since CP is not localized in replication-supporting spherules (30, 42), it is hard to reconcile a mechanism that offers a productive interaction between CP and the replication complex to upregulate plus-strand synthesis and promote replication-coupled packaging. In this study, immunofluorescence confocal microscopy (IFCM) was used to explore the subcel-

* Corresponding author. Mailing address: Department of Plant Pathology and Microbiology, University of California, Riverside, CA 92521-0122. Phone: (951) 827-3810. Fax: (951) 827-4294. E-mail: arao@ucr.edu.

▽ Published ahead of print on 5 January 2011.

lular localization sites of BMV CP synthesis. In addition, results of transmission electron microscopy (TEM) of whole plants either infected with wild-type (wt) BMV (mechanically and via agroinfiltration) or expressing CP ectopically revealed a collection of previously unrecognized ER membrane alterations. These observations offer a new perspective toward elucidation of CP-organized viral functions that are intimately linked to replication-coupled RNA packaging.

MATERIALS AND METHODS

Full-length BMV cDNA clones and CP-GFP fusion. Full-length cDNA clones of BMV genomic RNAs from which infectious RNAs can be transcribed *in vitro* have been described previously (15). To construct a recombinant plasmid competent to express CP-GFP (green fluorescent protein) fusion, a cDNA product encompassing the GFP coding region was amplified in a PCR using a forward primer (5′ CCGGTCGCCACCGAGGCCAAAGGAGAA [StuI site is underlined]) and a reverse primer (5′ TCGCTGATTATGAGAGGCCGTCGCGGC CGCT [StuI site is underlined]). The resulting product was digested with the restriction enzyme StuI and subcloned to a StuI-digested full-length clone of pT7B3. The presence of the subcloned GFP region in the desired orientation was confirmed by sequencing. The final recombinant plasmid is referred to as B3/CP-GFP (Fig. 1A).

T-DNA plasmids, agroinfiltration, and progeny analysis. The construction, characteristics, and biological activities of T-DNA plasmids corresponding to BMV genomic RNAs have been described previously (2, 4). Approximately 4-week-old *Nicotiana benthamiana* plants were agroinfiltrated using transformed *Agrobacterium tumefaciens* (strain GV 3101) culture at an optical density at 600 nm (OD_{600}) of 0.5 (2). RNA progeny analysis was performed as described previously (3).

Antisera and IFCM. Primary antibodies used were 1a and 2a (kindly provided by Paul Ahlquist, University of Wisconsin, Madison, WI), BMV CP (4), J2 mouse monoclonal anti-double-stranded RNA (dsRNA; 1:200; English & Scientific Consulting, Hungary), KDEL (Lys-Asp-Glu-Leu) mouse monoclonal antibody (antibody for KDEL motif; 1:100; Enzo Life Sciences), and rabbit anti-BiP antibody (1:50; Santa Cruz Biotechnology). Secondary antibody used for IFCM was either Alexa Fluor 633-conjugated anti-rabbit or anti-mouse antibody (1:100; Molecular Probes). For IFCM analysis, leaf segments were fixed and treated with the desired antibody as described previously (24). Confocal microscopy was performed as described previously (6).

Electron microscopy. For conventional TEM, *N. benthamiana* leaves were fixed and embedded in either Spurr's resin or LR White resin as described previously (5). For immunogold labeling, osmium tetroxide was omitted during fixation. Tissue sections of approximately 50 nm were mounted onto copper (for TEM) or nickel (for immunoelectron microscopy [IEM]) grids and then treated with the desired primary antibody and gold-conjugated secondary antibody as described previously (5). For simultaneous detection of two antigens, the silver enhancement-controlled sequential immunogold (SECSI) procedure (8) was used. Briefly, after the tissue was fixed and sectioned as described previously (5), sections were mounted onto nickel grids and placed in phosphate buffer (PB) containing 0.1% sodium borohydride to inactivate residual aldehyde groups. Following several washes in PB, the sections were incubated in PB containing 0.05% Triton X-100 to increase reagent penetrability. Then the samples were incubated for 1 h in a blocking solution (phosphate-buffered saline [PBS], pH 7.4, containing 5% preimmune serum, 5% bovine serum albumin [BSA], and 0.1% gelatin) followed by incubation in the primary antibody raised against the first antigen (i.e., 1a) diluted in PBS. Sections were then incubated in the F(ab′)2 goat anti-rabbit antibody gold conjugate (Ultra Small Gold; EM Sciences) followed by silver enhancement (using a kit from EM Sciences) for 12 to 15 min and fixed for 2 min in 3% sodium thiosulfate. Before the application of the antibody raised against the second antigen (i.e., 2a), sections were washed, and the procedure used for the first primary antibody was repeated. The sections were silver enhanced for 6 min, washed, and fixed in 2% glutaraldehyde to prevent the loss of gold-labeled antibody during the final staining process. After the grids were rinsed with sterile distilled water, they were stained with uranyl acetate and lead citrate for 30 min prior to viewing under the transmission electron microscope.

Statistical analysis. To quantify the extent of immunogold label associated with various organelles, the data were analyzed statistically as described previously (6). Analysis of variance (ANOVA) procedures with PC SAS version 9.0 (SAS Institute) and PROC GLM were used to evaluate differences in the numbers of gold particles observed in four locations (cell wall, cytoplasm, ER, and vesicles) in the electron micrographs. The analysis was performed for wt BMV-infected cells using 1a and 2a antisera and preimmune serum as a control. Due to problems in homogeneity of variance and distributional assumptions, a square-root transformation was used prior to conducting the ANOVAs. When the ANOVA was significant, Tukey's pairwise comparisons of the locations were made with a P value differences option in a least squares mean statement. A significance level of 0.05 was used for all comparisons.

RESULTS

BMV CP localizes to the ER. A preliminary study from our lab examined the distribution of *Cowpea chlorotic mottle virus* (CCMV) CP, another member of the *Bromoviridae* family, in three different host plants (35). In contrast to free GFP that was distributed throughout the cytoplasm, CCMV CP-GFP fusion was localized as punctate bodies in the cytoplasm, but the precise subcellular localization site for CCMV CP was not determined (35). Therefore, in this study, the application of IFCM in conjunction with antibodies specific for viral CP and cellular marker proteins allowed us to further characterize the precise subcellular localization of the BMV CP in plant cells. Consequently, a variant clone of BMV RNA3 (referred to as B3/CP-GFP) encoding CP as a GFP fusion was constructed (Fig. 1A). In the B3/CP-GFP construct, the N terminus of the GFP ORF was fused to the CP C terminus. It is anticipated that following translation of the protein from replication-derived sgmRNA, the resulting CP-GFP fusion would not assemble into virions. This is because in bromoviruses, an interaction between the N- and C-termini of CP is obligatory for dimer formation, a critical step toward virus assembly (57). *In vitro* transcripts of B3/CP-GFP were coinoculated with wt transcripts B1 (full-length BMV RNA1) and B2 (full-length BMV RNA2) to *Nicotiana benthamiana* leaves. As expected, B3/CP-GFP replicated to synthesize CP mRNA and expressed GFP (see below), but the fusion protein failed to assemble into virions (Fig. 1B). To monitor the subcellular localization of the GFP signal, leaves inoculated with B1+B2+B3/CP-GFP were subjected to IFCM. In contrast to the uniform distribution of free GFP throughout the cytoplasm (4), low-magnification images showed that cells expressing CP as a GFP fusion contained green fluorescence as punctate structures (Fig. 1C, panels a and d). Higher magnification revealed that each vesicular compartment was filled with fluorescence (Fig. 1C, panels 1 and 3). To identify the CP localization sites, immunofluorescence using primary antibodies against two ER markers, namely, KDEL motif (Lys-Asp-Glu-Leu) (56) or BiP (binding protein) (17), was performed with B1+B2+B3/CP-GFP-infected leaves. Following fixation of the leaves as described in Materials and Methods, incubation with Alexa Fluor 633-conjugated secondary antibodies (emitting red fluorescence) permitted dual localization of GFP and each ER marker protein by IFCM. Low- and high-magnification images are shown in Fig. 1C (panels b and c, e and f). Emission of red fluorescence in leaves treated with Alexa Fluor 633 identified the ER network (Fig. 1C, panels b and e). When both images were merged, most of the CP-GFP (~80%) coincided with the ER network, resulting in a yellow fluorescence (Fig. 1C, panels c and f). The remaining 20% of the CP-GFP lacked detectable KDEL or BiP colocalization (Fig. 1C, panels c and f; indicated by an arrowhead). These results suggested that a high proportion of the CP is associated with the ER.

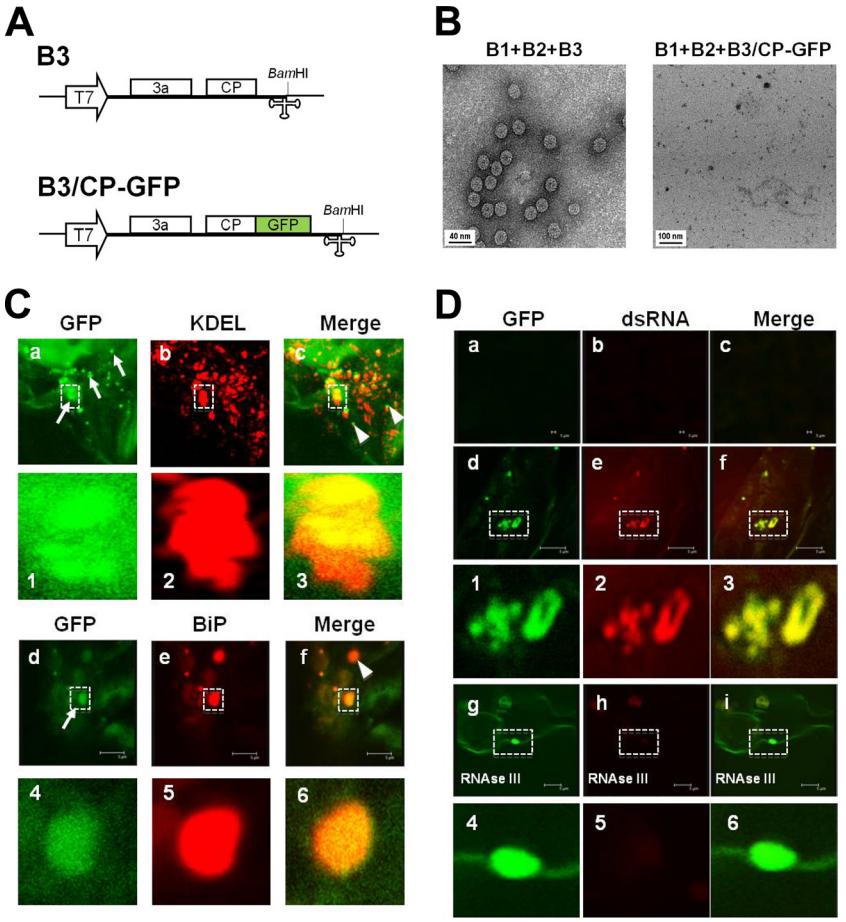

FIG. 1. Subcellular localization of BMV CP and replication sites. (A) Schematic representation of constructs used for *in vitro* transcription of wild-type BMV RNA3 (B3) and its chimera, B3/CP-GFP, designed to express GFP as a CP fusion protein. White boxes represent movement protein (3a) and CP ORFs. The position of the BamHI site used to linearize the plasmids for *in vitro* transcription using T7 polymerase is indicated. (B) TEM images of virions purified from *N. benthamiana* plants mechanically inoculated with the indicated inocula. (C) Subcellular localization of BMV CP. *N. benthamiana* leaves were mechanically inoculated with B1+B2+B3/CP-GFP inoculum and processed for IFCM. Antisera to ER-resident proteins KDEL and BiP were used to label ER followed by treatment with Alexa Fluor 633-conjugated secondary antibodies (emits red fluorescence). (Ca and Cd) Infected leaf cells showing aggregates of CP-GFP fusion as punctate bodies (indicated by arrows); (Cb and Ce) red fluorescence indicates ER; (Cc and Cf) yellow fluorescence in merged images represents where CP and ER colocalize; absence of yellow signal, representing noncolocalized areas, is indicated by arrowheads. Cellular regions boxed in panels a to c and d to f are shown enlarged in panels 1 to 3 and 4 to 6, respectively. (D) Colocalization of BMV CP and replication sites. Mock (Da to Dc)- or B1+B2+B3/CP-GFP (Dd to Df)-infected *N. benthamiana* leaves were probed for the presence of dsRNA using monoclonal antibody J2 and then treated with Alexa Fluor 633-conjugated secondary antibody. Green and red fluorescence in panels d and e, respectively, represent localization of the CP-GFP fusion protein and replication sites. Yellow fluorescence in panel f represents where CP and dsRNA colocalize. The cellular region boxed in panels d to f is shown enlarged in panels 1 to 3, respectively. (Dg and Dh) Infected leaves were treated with RNase III and probed for dsRNA. The cellular region boxed in panels g to i is shown enlarged in panels 4 to 6, respectively. Bars, 5 μm.

Subcellular localization sites of BMV CP and viral replication overlap. It has previously been shown that BMV replication occurs in ER-derived spherule invaginations (30, 42). Since genome packaging in BMV is functionally coupled to replication (3), we performed the following experiment to verify whether subcellular localization sites of replication and CP integrate or segregate. Double-stranded RNA (dsRNA) is a generally accepted marker for intermediates during replication of positive-strand RNA viruses (51, 52). Monoclonal antibody J2 has been shown to specifically recognize dsRNA of more than 40 bp in length, and the antibody binding is independent of sequence and nucleotide composition of the antigen (41). Consequently, the J2 antibody has been successfully used to visualize dsRNA in cells infected with a number of positive-strand RNA viruses (23, 47, 52, 55). Therefore, *N. benthamiana* leaves inoculated with B1+B2+B3/CP-GFP were processed for the dsRNA detection using the J2 antibody by IFCM. Results are shown in Fig. 1D. Treatment of healthy control leaves with the J2 antibody did not reveal any fluorescence signal (Fig. 1D, panels a to c). Replication of B1+B2+B3/CP-GFP was confirmed by detection of the GFP signal (Fig. 1D, panels d and 1). In these leaves, the J2 antibody signal, representing BMV replication sites, appeared as discrete red fluorescent foci in the cytoplasm (Fig. 1D, panels e and 2). Merging of the two images resulted in the yellow fluorescence (Fig. 1D, panels f and 3), indicating that CP is colocalized to replication sites.

To determine whether the red fluorescent foci detected by

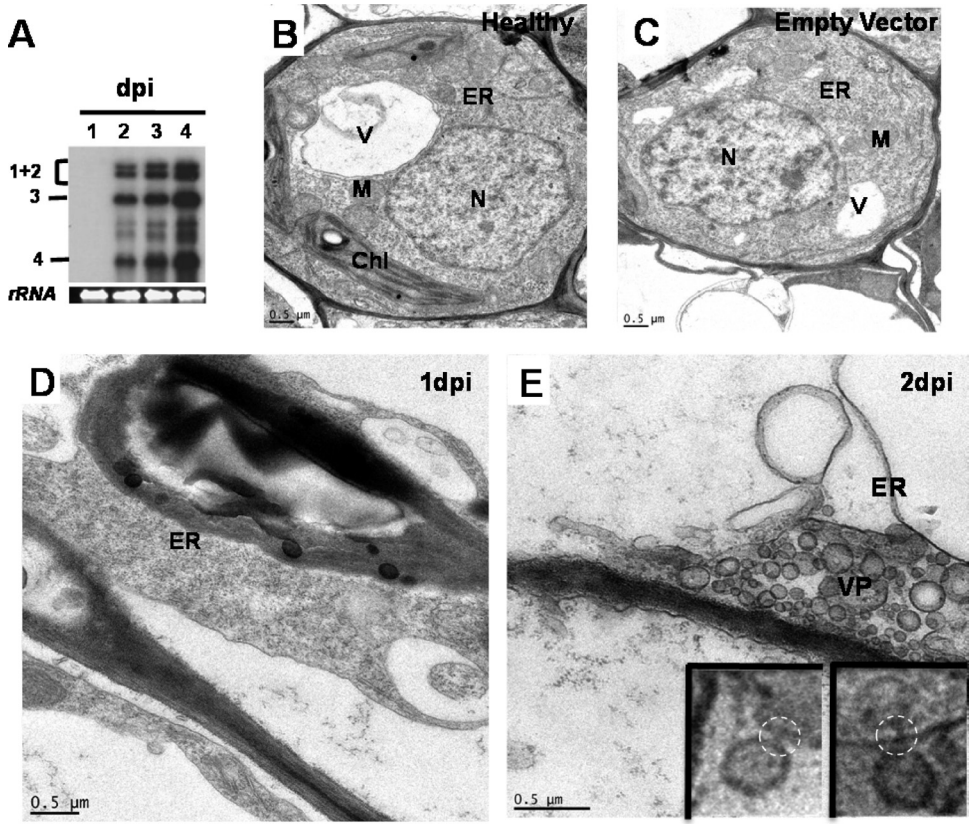

FIG. 2. BMV replication correlates with vesicle induction in *N. benthamiana* leaves. (A) Temporal pattern of BMV RNA accumulation in *N. benthamiana* leaves infiltrated with agrotransformants of all three wt BMV RNAs. Northern blot showing the accumulation of BMV progeny RNA in leaves at 1 to 4 days postinfiltration (dpi). Five micrograms of total RNA per sample was subjected to fractionation on denaturing formaldehyde-agarose gels, transferred to a nylon membrane, and hybridized with a ^{32}P-labeled riboprobe complementary to a sequence encompassing the conserved 3′ tRNA-like structure that detected all four BMV RNAs. The positions of the four BMV RNAs are indicated on the left. (B to E) BMV infection induces ultrastructural changes to the ER membrane. *N. benthamiana* leaves at various dpi were fixed, sectioned, and stained with uranyl acetate and analyzed by TEM. TEM images of a cell from healthy (B) and empty vector-infiltrated (C) leaves showing distribution of unmodified nucleus (N), endoplasmic reticulum (ER), vacuole (V), chloroplast (Chl), and mitochondria (M). (D) At 1 dpi, no change to any cellular organelle was observed. (E) A TEM image showing the formation of a vesicle packet (VP) containing a collection of virus-induced vesicles surrounded by ER at 2 dpi. (Insets) A magnified view of a vesicle as observed in many sections, showing a neck (dotted circle) connecting to ER. Bars, 0.5 μm.

the J2 antibody contained dsRNA, *N. benthamiana* leaves infected with B1+B2+B3/CP-GFP were treated with RNase III (specific for dsRNA). As expected, red fluorescence signal emitted by the J2 antibody was completely lost after the RNase III treatment (Fig. 1D, panels h and 5) while the GFP signal of the CP-GFP fusion remained unaffected (Fig. 1D, panels g, i, 4, and 6). Taken together, these results confirmed that the sites of CP synthesis and viral replication overlap.

TEM analysis of BMV-infected plant cells reveals accumulation of distinct membrane structures. IFCM data presented above (Fig. 1D) clearly showed that sites of CP synthesis and viral replication are integrated. Furthermore, since BMV CP has been shown to affect strand asymmetry (9, 26), we reasoned that CP might function in close association with replication-supporting spherule invaginations. To examine this possibility, we used TEM to visualize membrane modifications induced by wt BMV in *N. benthamiana* leaves. Consequently, to achieve synchronized entry to the same cell (4), a constellation of all three wt BMV RNA agroconstructs was infiltrated into *N. benthamiana* leaves and harvested at various days postinfiltration (dpi). Infiltrated leaves were divided into two lots. The first lot was used to analyze the accumulation of progeny RNA by Northern analysis, whereas the second lot was processed for TEM analysis. Results of Northern analysis of BMV progeny accumulating at various dpi are shown in Fig. 2A. The first signal of progeny RNA detection was evident at 2 dpi but not 1 dpi (Fig. 2A). This delay in BMV progeny RNA detection could be attributed to a lapse in time taken to transfer transgenes from the T-DNA region of the bacterial Ti plasmid into the plant nucleus followed by transient expression. From 2 dpi onward, the progeny RNA continued to accumulate with time (Fig. 2A).

TEM analysis of *N. benthamiana* leaves from healthy, empty-vector-infiltrated, and BMV-infected plants at 1 to 4 dpi are shown in Fig. 2 and 3. Similar to the healthy control (Fig. 2B), ER, nucleus, mitochondria, and chloroplasts appeared normal in leaves infiltrated with empty vector (Fig. 2C), suggesting that agrobacterium had no detectable effect on any of the cellular organelles. The absence of detectable viral replication at 1 dpi (Fig. 2A) correlated with the absence of any noticeable changes in the structure of intracellular membranes and organelles (Fig. 2D). However, at 2 dpi, the time at which rep-

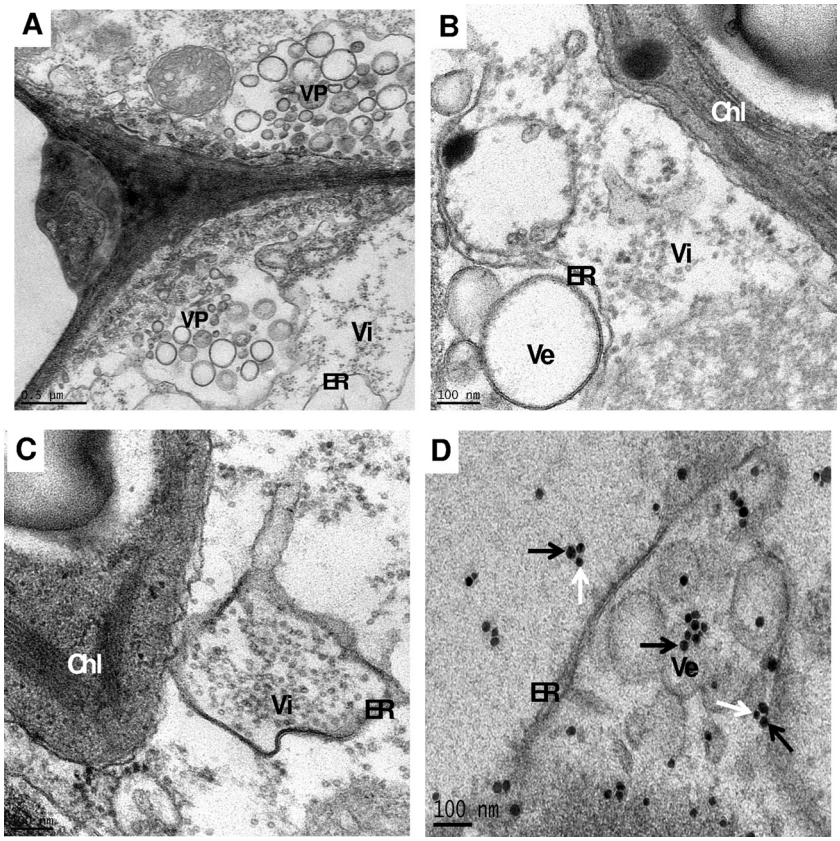

FIG. 3. Ultrastructure of distinct membrane alterations induced by BMV in *N. benthamiana* leaves at 4 dpi. A collection of TEM images of BMV-infected leaves fixed at 4 dpi are shown in panels A to C. (A) An overview of two neighboring cells infected by BMV showing a collection of virus-induced vesicles in the lumen of the ER to form a vesicle packet (VP). Assembled virions (Vi) are found scattered in the vicinity of VP. (B) An example of distinct cytopathological change induced by BMV infection showing accumulation of vesicles (Ve); (C) a higher-ordered ER structure accumulating assembled virions; (D) immunogold localization of viral replicase proteins 1a and 2a to vesicles in BMV-infected cells. Following fixation of leaf tissue, thin sections were labeled with antibodies specific to replicase proteins 1a and 2a using the SECSI technique (see Materials and Methods). Black and white arrows, respectively, represent 1a and 2a. Bars, 0.5 μm (A) and 100 nm (B to D).

licated BMV progeny RNA was first detected (Fig. 2A), accumulation of a large cluster of vesicles into membrane sacs, which we refer to as vesicle packets (VPs), was readily observed (Fig. 2E). These VPs are absent in healthy leaves or leaves infiltrated with empty vector (Fig. 2B and C). The vesicles were globular in shape and displayed polymorphism, with diameters ranging between 33 and 267 nm. A closer examination further revealed a few spherule-like structures whose outer membrane appeared to connect to the ER through narrow necklike connections (see insets in Fig. 2E). The VPs were clearly associated with extensively dilated ER (Fig. 2E). Except for ER, other cellular organelles, such as mitochondria and chloroplasts, appeared normal. At 3 dpi, as the viral replication continued to increase with time (Fig. 2A), vesicle accumulation was also increased (data not shown). At 4 dpi, when the replication progeny accumulation was the highest compared to that at other dpi (Fig. 2A), large assemblies of vesicle clusters were observed (Fig. 3A). These vesicles were organized into large VPs surrounded by the ER. A representative example can be seen in Fig. 3B. In addition to VPs, structures resembling assembled virions were also detected, and their concentration varied with time, the least being at 2 dpi (Fig. 2E) and the highest being at 4 dpi (Fig. 3A to C). In some sections, virion-like structures were found in the lumen of the modified ER (Fig. 3C). However, unlike in yeast cells supporting BMV replication (42), vesicle induction in the perinuclear region was never observed (see Discussion for an explanation).

To further evaluate whether vesicle clusters present in VP support viral replication, we employed immunogold labeling. Thin sections of wt BMV-infected and healthy *N. benthamiana* leaves were simultaneously treated with both 1a and 2a antisera using the silver enhancement-controlled sequential immunogold (SECSI) technique. Immunogold labeling patterns were analyzed by TEM to assess the distribution of gold particles in various subcellular compartments and virus-induced vesicles. A representative example of a TEM image is shown in Fig. 3D. Gold particles for 1a (large size indicated by black arrow in Fig. 3D) and 2a (small size indicated by white arrow in Fig. 3D) were counted in 10-μm^2 fields and were scored for their association with cell wall, cytoplasm, ER, and vesicles. The average numbers of gold particles labeling cell wall, cytoplasm, ER, and vesicles are shown in Table 1. The analysis revealed that a significant amount of immunogold labeling detecting 1a was associated with vesicles (46%) and ER (24%) compared to other locations (Table 1). Previous studies found that in BMV and genetically related *Cucumber mosaic virus*

TABLE 1. Distribution of immunogold labeling of anti-1a and anti-2a antisera in *N. benthamiana* leaves infected with wt BMV[a]

Treatment	No. of fields	No. (±SE) of gold particles in:			
		Cell wall	Cytoplasm	ER	Vesicles
Anti-1a antiserum	25	0.4 ± 0.22 B	0.72 ± 0.20 AB	0.88 ± 0.21 AB	**1.68 ± 0.34 A**
Anti-2a antiserum	25	0.28 ± 0.11 B	1.04 ± 0.29 B	**1.96 ± 0.43 A**	1 ± 0.29 B
Preimmune antiserum	25	0.00 ± 0.00 B	0.28 ± 0.09 A	0.08 ± 0.06 B	0.00 ± 0.00 B

[a] Resin-embedded leaves of *N. benthamiana* infected with wt BMV were sectioned and analyzed by immunogold labeling by using the SECSI technique to assess the subcellular distribution of BMV 1a and 2a. Immunogold labeling was performed as described in Materials and Methods. Fields are defined as 10-μm^2 areas (using an ultrastructural size calculator) that contain gold particles. Gold particles in each field were counted manually. Although the application of SECSI technique involves the use of a mixture containing two antisera, for clarity the data are shown for each antiserum. Zeros indicate subcellular domains with no label. Statistical analysis was conducted as detailed in Materials and Methods. Bolded values represent the values that show the greatest amount of immunogold label (compared to other values in the same rows) and that are significantly above zero. Different letters next to each standard error represent statistical significant differences. Note that values with the same letter are not significantly different.

(CMV), unlike 1a, 2a has been present in both membrane and cytoplasmic fractions (10, 42). Consequently, our immunogold labeling detecting 2a was associated with membranes (46% with ER and 23% with ER-derived vesicles), while 24% was associated with cytoplasm (Table 1). Taken together, these labeling patterns of 1a and 2a observed in this study are in agreement with previously published reports (10, 42).

Agroinfiltration is a versatile approach for the synchronized delivery of multiple components to the same cell (2, 4), resulting in the onset of robust replication, compared to mechanical inoculation, where synchronized delivery is uncontrollable. Thus, to verify whether the observed ultrastructural modifications seen in agroinfiltrated leaves are not due to the onset of agroinfiltration-mediated robust replication, *N. benthamiana* leaves were mechanically inoculated with all three wt BMV transcripts and harvested at various days postinoculation, and progeny RNA accumulation was analyzed by Northern blot hybridization followed by TEM analysis. Results are shown in Fig. 4. In contrast to agroinfiltration, the inherent inefficient synchronized delivery of all three BMV components to the same cell by mechanical inoculation resulted in a slower onset of BMV replication and accumulation of progeny RNA (compare Fig. 2A and 4A). However, TEM examination of mechanically inoculated leaves revealed the accumulation of a cluster of vesicles into membrane sacs (Fig. 4) similar to those seen in agroinfiltrated leaves (Fig. 2E and 3A to D). Representative examples of TEM images showing membrane alterations induced in four independent cells of mechanically inoculated leaves are shown in Fig. 4B to E. These observations substantiate that ultrastructural modifications induced by BMV in mechanically inoculated and agroinfiltrated leaves are indistinguishable.

Three distinct types of vesicles are found in BMV infection. A closer examination of thin-section EM analysis of VP induced in leaves agroinfiltrated with wt BMV revealed the presence of three vesicle types (Fig. 5A). Type 1 measured 66 nm ± 3.1 nm in diameter and contained electron-dense fibrillar material reminiscent of nucleic acid (Fig. 5B). Type 2 vesicles measured 359 nm ± 4.6 nm in diameter, but the interior contained little or no electron-dense material (Fig. 5C) and resembled those induced exclusively by CP (see below). Morphological features of type 3 vesicles are clearly distinct from those of types 1 and 2 (Fig. 5D). Type 3 vesicles had a diameter of 310 nm ± 2.3 nm and are partly surrounded by an ER membrane (indicated by arrows in Fig. 5D). The interior of type 3 vesicles always contained highly stainable electron-dense material. Another distinguishing feature characteristic of type 3 vesicles is the presence of an internal vesicle bound with a single membrane (indicated by a single arrow in Fig. 5D). This internal vesicle often contained darkly stained globular structures, whose identity remains to be established. Based on these features, we speculate that vesicles of type 3

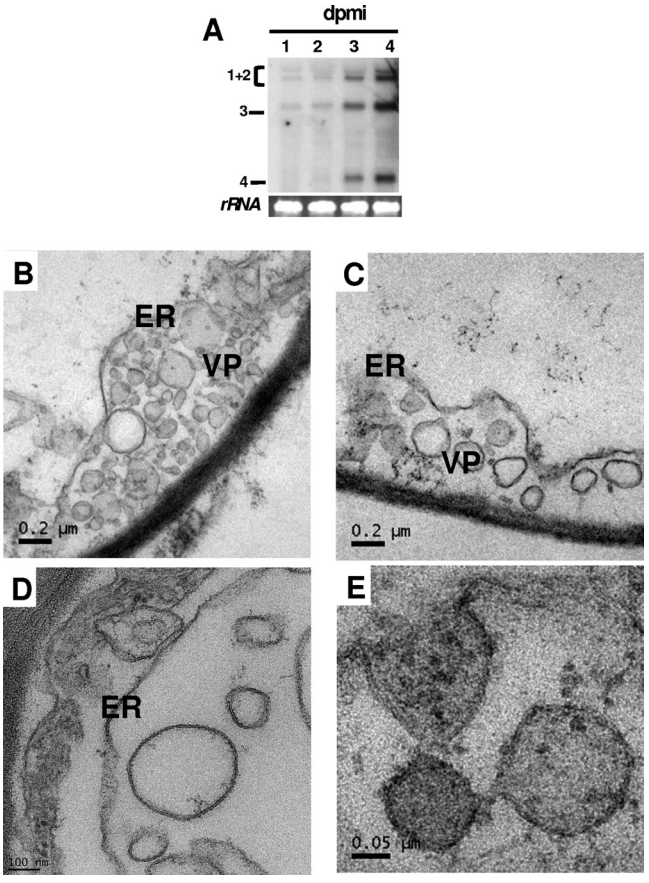

FIG. 4. Ultrastructure of membrane alterations induced by wt BMV infection in mechanically inoculated *N. benthamiana* leaves. (A) Northern blot showing the temporal pattern of BMV RNA accumulation at 1 to 4 days postmechanical inoculation (dpmi). (B to E) Representative TEM images showing the accumulation of vesicles in leaves at 3 dpmi. Bars, 0.2 μm (B and C), 100 nm (D), and 0.05 μm (E).

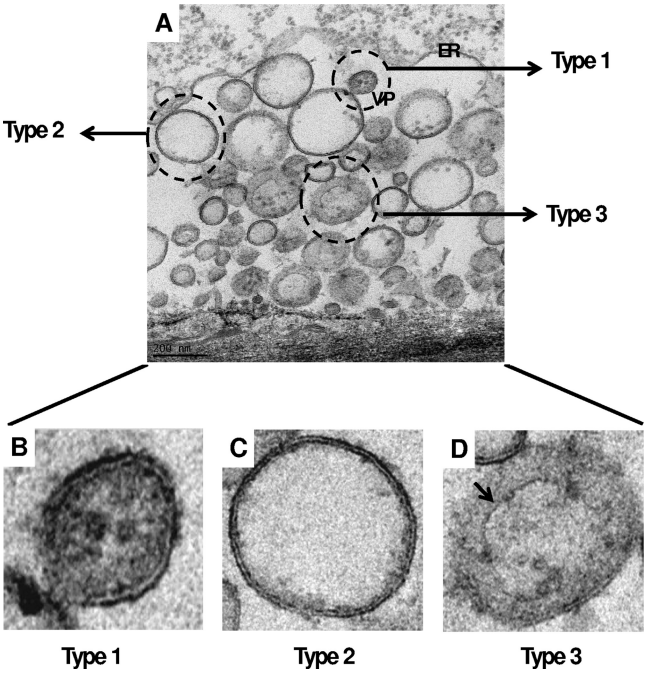

FIG. 5. Types of vesicles associated with wt BMV infection. (A) An overview of vesicles accumulated in *N. benthamiana* leaves following agroinfiltration with wt BMV. Representative examples of three vesicle types, classified as type 1, 2, and 3, are indicated. Higher-magnified views of each vesicle type are shown in panels B to D. Note in panel D, the outer wall membrane is not continuous. An arrow indicates the internal structure with a single outer membrane. Bars, 200 nm.

result from fusion between type 1 and type 2. The three types of vesicles were seen in ER-derived VPs as early as 2 dpi. At this time point, VPs exhibited the propensity to accumulate on the cell wall near plasmodesmata (PD). In addition to wt BMV infection, the induction of each of the three types of vesicles is associated with expression of a given viral protein (see below).

Ectopic expression of CP results in vesicle induction. Previous TEM analysis of yeast cells expressing all four BMV genes individually, together, and in all pairwise combinations revealed that 1a alone was necessary and sufficient to induce spherules, and 2a, CP, or other BMV genes were not required (42). To verify whether this is the case with plants, *N. benthamiana* leaves were infiltrated with agroconstructs of B1, B2, and B3 individually to express 1a, 2a, and 3a, respectively, and three pairwise combinations (i.e., B1 plus B2; B1 plus B3, and B2 plus B3). In addition, plants were infiltrated only with a B4 agroconstruct that had previously been shown to express CP in the absence of BMV replication (4). In each case, leaves were harvested at various dpi and processed for TEM examination, and representative electron micrographs are shown in Fig. 6.

As observed in yeast cells, ectopic expression of 1a (Fig. 6A), but not 2a (Fig. 6B) or 3a (Fig. 6C), resulted in the induction of vesicles derived from ER. After infiltration with the three pairwise combinations, as observed in yeast cells, vesicle induction was seen for B1 plus B2 (Fig. 6D and E) and B1 plus B3 but not for B2 plus B3 (data not shown). Interestingly, vesicles induced by B1 plus B2 are engulfed by the modified ER into a VP (Fig. 6D and E), similar to those seen in wt BMV infection (Fig. 2E and 3A). However, unlike in yeast cells, vesicles induced by only 1a are not perinuclear and appear to be derived from cytoplasmic ER (also see Discussion). Additional immunogold-EM analysis using anti-dsRNA confirmed that vesicles induced by B1 plus B2 are the sites of viral replication (Fig. 6E).

A surprising result, in marked contrast to that of yeast cells, emerged when the BMV CP was expressed in isolation. We found that, in the absence of other viral genes, CP alone was sufficient to induce large numbers of vesicles arranged into VPs (Fig. 7). At 2 dpi, VPs containing a large cluster of polymorphic vesicles with a diameter of 23 to 605 nm were observed in the perinuclear area (Fig. 7A). By 4 dpi, most of the VPs moved away from the perinuclear region, concentrating on either side of the cell wall (Fig. 7B), and are frequently seen close to plasmodesmata, as shown in Fig. 7B. Unlike VP induced by wt BMV infection that contained three vesicle types, VPs resulting from ectopic expression of CP contained only vesicles of type 2 but not type 1 or type 3.

BMV CP-induced vesicles are ER derived. TEM analysis suggested that CP-induced vesicles in resin-embedded leaf tissue are likely derived from the ER. To verify this assumption, immunogold EM with antibodies to BiP, an ER marker protein, was employed. The outer membrane of VP induced by CP (Fig. 8A) and vesicles found within this VP (Fig. 8B) are clearly and specifically labeled for the BiP. Immunogold EM localization of CP revealed labeling of anti-BMV CP antibody on ER membranes, including CP-induced vesicles (Fig. 8C and D). In addition, labeling of anti-BMV CP antibody was also observed in the cytoplasm, perhaps detecting CP in the form of assembled virions since ectopically expressed CP is competent for virion assembly (4). Collectively, these data suggested that vesicles induced by CP are ER derived.

DISCUSSION

Using intact *N. benthamiana* plants as a model host organism, in conjunction with IFMC analysis of the CP-GFP fusion protein, we provide evidence that the sites of BMV CP synthesis and viral replication overlap and are localized to large vesicular compartments derived from the ER (Fig. 1C and D). We extended our analysis of wt BMV-infected *N. benthamiana* leaves to the ultrastructural level by TEM and identified distinct membrane structures (Fig. 2 and 3), similar to those observed in cells infected with SARS-coronavirus and dengue-flavivirus (44, 54). The most striking and major result of this work is that ectopic expression of BMV CP has exhibited an intrinsic property of modifying ER and inducing vesicles similar to those present in whole-virus infections (Fig. 7). As discussed below, the reticulovesicular network of ER modified by the wt BMV infection along with that induced by the ectopic expression of CP places the intrinsic involvement of CP in upregulating plus-strand synthesis and promoting replication-coupled packaging in a new perspective.

Subcellular localization sites of BMV CP. Although the subcellular localization sites for BMV RNA synthesis have been delineated (37, 42), those of the CP remained elusive. The subcellular localization of the CP was previously visualized by TEM as virus particles for BMV and other icosahedral plant RNA viruses (16). In these previous studies, tissues obtained

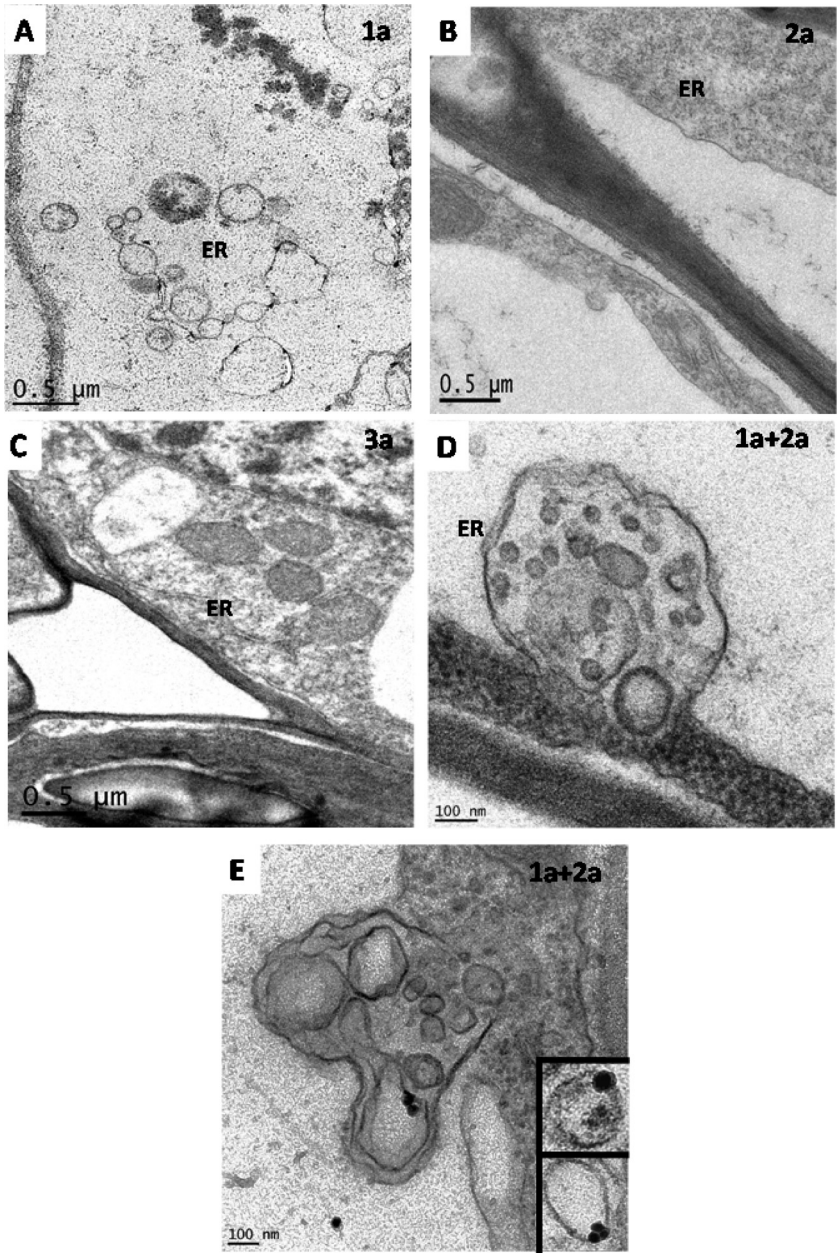

FIG. 6. Ectopic expression of BMV gene products. TEM images of leaf sections following ectopic expression of BMV replicase genes 1a (A) and 2a (B) and movement protein 3a (C) are shown. No change to any cellular organelle was observed in leaves infiltrated with either 2a (B) or 3a (C). (D) Accumulation of vesicles and formation of VP following coinfiltration with 1a and 2a. (E) Representative TEM image showing immunogold localization of dsRNA in vesicles induced by 1a plus 2a. (Inset) dsRNA localization on vesicles induced by 1a plus 2a from different tissue sections. Bars, 0.5 μm (A to C) and 100 nm (D and E).

from 2- to 3-week-old systemically infected leaves were used, and in each case, virions were found to be scattered throughout the cytoplasm of the cell (16). In the present study, the application of IFCM to *N. benthamiana* leaves inoculated with B1+B2+B3/CP-GFP showed that the CP translated from replication-derived mRNA not only localized on the ER but coaligned with sites of viral replication (Fig. 1). A similar scenario was recently observed for FHV CP, which was localized to mitochondria where FHV RNA replication occurs (49). It was found that trafficking of FHV CP to replication sites (i.e., mitochondria) is determined by the N-terminal arginine-rich motif (ARM). Like FHV, CPs of BMV and several plant-infecting icosahedral RNA viruses (36) and HIV Tat protein (46) contain ARMs that have been implicated in RNA binding and selective RNA packaging (12). Therefore, the newly recognized additional role of the ARM of the viral CP in subcellular trafficking is of relevance to this study. In our study, ectopic expression experiments revealed that BMV CP itself has the intrinsic property of modifying ER (Fig. 7) to induce vesicles. Therefore, like FHV, the ARM of BMV CP might

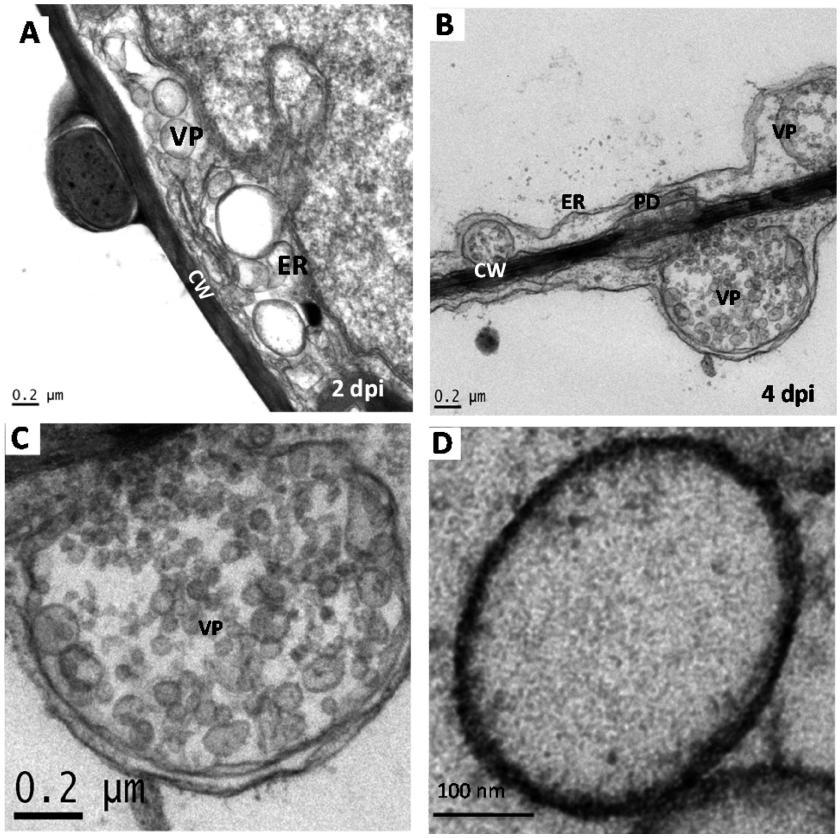

FIG. 7. Ectopic expression of BMV CP results in vesicle induction. TEM images showing induction of a collection of vesicles in *N. benthamiana* leaves ectopically expressing BMV CP at 2 dpi (A) and 4 dpi (B). A magnified view of a VP containing a collection of vesicles induced by CP in ER lumen is shown in panel C. A magnified view of a CP-induced vesicle is shown in panel D. Bars, 0.2 μm (A to C) and 100 nm (D).

have an ER localization signal. Since FHV can replicate in plant cells (5), subcellular localization of hybrid constructs of BMV and FHV having a heterologous ARM in conjunction with the mutational analysis of BMV CP ARM is likely to shed more light on the precise role of the ARM in subcellular trafficking.

Possible roles of CP-induced vesicles in the BMV life cycle. Previous TEM studies of bromovirus-infected plant tissue reported proliferation of the ER membranes into vesicles (16, 20, 32). In these early studies performed nearly 3 decades ago, use of systemically infected leaves (~2 to 3 weeks postinoculation) for TEM analysis, inability to ectopically express individual viral gene products, and the lack of sensitive, organelle-specific markers (e.g., anti-KDEL or anti-BiP) failed to conclusively link the functional relationship of vesicle induction to infection and disease progression. The advent of a genetically well-characterized surrogate yeast system provided novel insights in understanding the role of host proteins and cellular membrane reorganization during replication of positive-strand RNA viruses (7, 27, 42). However, the present study using an intact *N. benthamiana* plant as a host system revealed at least two distinct cytopathological changes associated with BMV infection that have not been observed in the surrogate yeast system. These are (i) accumulation of VP containing a collection of three types of vesicles (Fig. 3A), similar to those observed in SARS and dengue virus infections (44, 54), and (ii) induction of vesicles in cells ectopically expressing CP (Fig. 7). It is likely that these differences could be due to different host systems used (yeast versus *N. benthamiana*) or variation in relative replication efficiency and protein expression levels in each respective system. Most importantly, the distinct organization of the ER in whole plant (45) versus unicellular yeast cells (50) could be the primary contributing factor for the observed variation in cytopathological changes. Plant ER is the most extensive, versatile, and adaptable organelle with large numbers of discrete functional domains (45). In plants, the ER, a part of the endomembrane system and membranes of secretory pathways, forms a dynamic network, the organization of which changes during the cell cycle and development (45). Furthermore, in plants, all ER membranes (rough ER, smooth ER, and nuclear envelopes) are physically linked and enclose a single, continuous lumen that extends beyond the boundaries of individual cells via the plasmodesmata (PD) (45) that plays a crucial role in virus transport between cells. Therefore, organization of the ER network in a given host system could have profound influence on how RNA viruses remodel the ER to induce structures specialized for a wide range of viral functions, including replication, packaging, movement, and pathogenesis.

In our TEM images, vesicle types 1 to 3 appear to be clustered and integrated into the modified ER (Fig. 3A). Since type 3 vesicles lack defined membrane structures throughout,

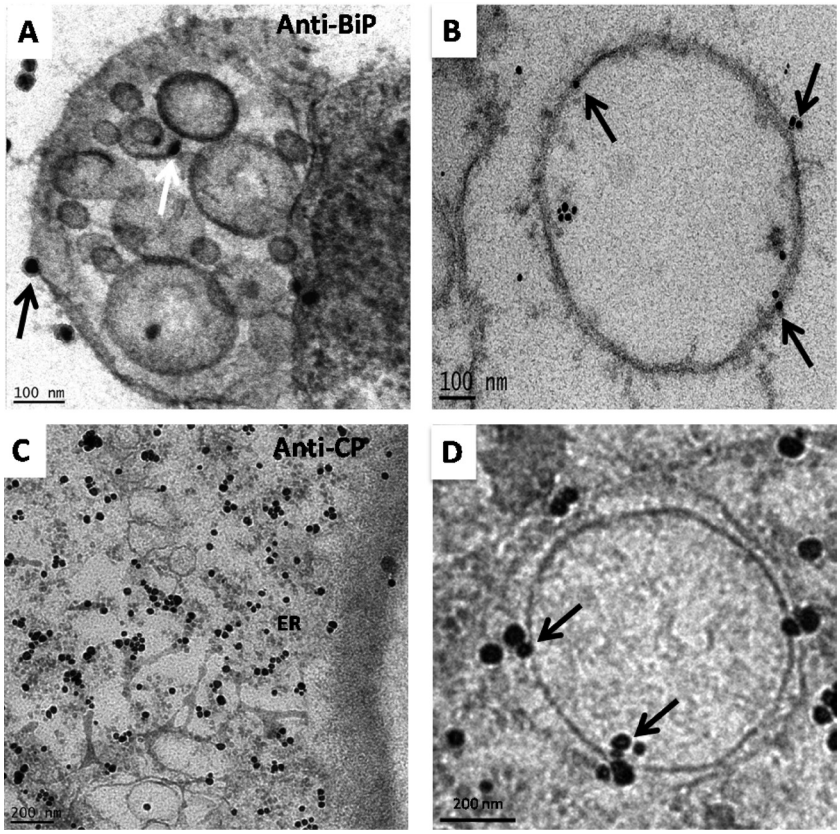

FIG. 8. Origin of CP-induced vesicles. (A) Leaf tissue ectopically expressing BMV CP was fixed and labeled with antibodies specific to BiP, an ER resident protein. Localization of BiP on the ER membrane surrounding CP-induced VP (black arrow) and on one of the vesicles (white arrow) is indicated. (B) An image showing a CP-induced vesicle labeled with BiP antibody (indicated by arrows). (C) Immunogold localization of anti-BMV CP in leaf tissue ectopically expressing BMV CP. (D) Magnified view of a CP-induced vesicle labeled with anti-BMV CP antibody (indicated by arrows) is shown. Bars, 100 nm (A and B) and 200 nm (C and D).

our routine chemical fixation procedure failed to preserve their ultrastructure for high-resolution analysis of connecting reticulovesicular network and immunogold localization studies to evaluate their involvement in replication. We are optimizing a freeze substitution technique for detailed characterization of type 3 vesicles and possibly unnoticed structural connections among three vesicle types using electron tomography. Such studies will shed light on the role of vesicles induced by replicase and CP in BMV replication and packaging.

ACKNOWLEDGMENTS

We thank Paul Ahlquist for the generous gift of 1a and 2a antibodies, Theo Dreher and Natasha Raikhel for helpful discussions, Deb Mathews for editorial comments, David Carter of the Center for Plant Cell Biology for assistance with confocal immunofluorescence microscopy, Advanced Center for Microscopy for use of TEM, and Santanu Datta of Department of Statistics for analyzing immunogold data.

Research in this laboratory was supported by a grant from the National Institutes of Health (1R21AI82301).

REFERENCES

1. **Ahlquist, P.** 2006. Parallels among positive-strand RNA viruses, reverse-transcribing viruses and double-stranded RNA viruses. Nat. Rev. Microbiol. **4:**371–382.
2. **Annamalai, P., and A. L. Rao.** 2006. Delivery and expression of functional viral RNA genomes in planta by agroinfiltration, unit 16B, p. 2.1–2.15. *In* T. Downey (ed.), Current protocols in microbiology. John Wiley & Sons Inc., Mississauga, Ontario, Canada.
3. **Annamalai, P., and A. L. Rao.** 2006. Packaging of brome mosaic virus subgenomic RNA is functionally coupled to replication-dependent transcription and translation of coat protein. J. Virol. **80:**10096–10108.
4. **Annamalai, P., and A. L. Rao.** 2005. Replication-independent expression of genome components and capsid protein of brome mosaic virus in planta: a functional role for viral replicase in RNA packaging. Virology **338:**96–111.
5. **Annamalai, P., F. Rofail, D. A. Demason, and A. L. Rao.** 2008. Replication-coupled packaging mechanism in positive-strand RNA viruses: synchronized coexpression of functional multigenome RNA components of an animal and a plant virus in *Nicotiana benthamiana* cells by agroinfiltration. J. Virol. **82:**1484–1495.
6. **Bamunusinghe, D., et al.** 2009. Analysis of potato virus X replicase and TGBp3 subcellular locations. Virology **393:**272–285.
7. **Barajas, D., Y. Jiang, and P. D. Nagy.** 2009. A unique role for the host ESCRT proteins in replication of tomato bushy stunt virus. PLoS Pathog. **5:**e1000705.
8. **Bienz, K., and D. Egger.** 1998. Electron microscopic-silver enhancement for double labeling with antibodies raised in the same species. Methods Mol. Biol. **80:**313–318.
9. **Bol, J. F.** 2008. Role of capsid proteins. Methods Mol. Biol. **451:**21–31.
10. **Chen, J., and P. Ahlquist.** 2000. Brome mosaic virus polymerase-like protein 2a is directed to the endoplasmic reticulum by helicase-like viral protein 1a. J. Virol. **74:**4310–4318.
11. **Chen, J., A. Noueiry, and P. Ahlquist.** 2003. An alternate pathway for recruiting template RNA to the brome mosaic virus RNA replication complex. J. Virol. **77:**2568–2577.
12. **Choi, Y. G., G. L. Grantham, and A. L. Rao.** 2000. Molecular studies on bromovirus capsid protein. VI. Contributions of the N-terminal arginine-rich motif of BMV capsid protein to virion stability and RNA packaging. Virology **270:**377–385.
13. **Denison, M. R.** 2008. Seeking membranes: positive-strand RNA virus replication complexes. PLoS Biol. **6:**e270.
14. **Diaz, A., X. Wang, and P. Ahlquist.** 2010. Membrane-shaping host reticulon

proteins play crucial roles in viral RNA replication compartment formation and function. Proc. Natl. Acad. Sci. U. S. A. **107:**16291–16296.
15. **Dreher, T. W., A. L. Rao, and T. C. Hall.** 1989. Replication in vivo of mutant brome mosaic virus RNAs defective in aminoacylation. J. Mol. Biol. **206:** 425–438.
16. **Francki, R. I. B., R. G. Milne, and T. Hatta.** 1985. Atlas of plant viruses, vol. II. CRC Press, Inc., Boca Raton, FL.
17. **Gething, M. J.** 1999. Role and regulation of the ER chaperone BiP. Semin. Cell Dev. Biol. **10:**465–472.
18. **Hull, R.** 2002. Plant virology, fourth ed. Academic Press, San Diego, CA.
19. **Khromykh, A. A., A. N. Varnavski, P. L. Sedlak, and E. G. Westaway.** 2001. Coupling between replication and packaging of flavivirus RNA: evidence derived from the use of DNA-based full-length cDNA clones of Kunjin virus. J. Virol. **75:**4633–4640.
20. **Kim, K. S.** 1977. An ultrastructural study of inclusions and disease development in plant cells infected by cowpea chlorotic mottle virus. J. Gen. Virol. **35:**535–543.
21. **Kujala, P., et al.** 2001. Biogenesis of the Semliki Forest virus RNA replication complex. J. Virol. **75:**3873–3884.
22. **Laliberte, J. F., and H. Sanfacon.** 2010. Cellular remodeling during plant virus infection. Annu. Rev. Phytopathol. **48:**69–91.
23. **Lee, J. Y., J. A. Marshall, and D. S. Bowden.** 1994. Characterization of rubella virus replication complexes using antibodies to double-stranded RNA. Virology **200:**307–312.
24. **Liu, J. Z., E. B. Blancaflor, and R. S. Nelson.** 2005. The tobacco mosaic virus 126-kilodalton protein, a constituent of the virus replication complex, alone or within the complex aligns with and traffics along microfilaments. Plant Physiol. **138:**1853–1865.
25. **Mackenzie, J.** 2005. Wrapping things up about virus RNA replication. Traffic **6:**967–977.
26. **Marsh, L. E., C. C. Huntley, G. P. Pogue, J. P. Connell, and T. C. Hall.** 1991. Regulation of (+):(–)-strand asymmetry in replication of brome mosaic virus RNA. Virology **182:**76–83.
27. **Miller, D. J., and P. Ahlquist.** 2002. Flock house virus RNA polymerase is a transmembrane protein with amino-terminal sequences sufficient for mitochondrial localization and membrane insertion. J. Virol. **76:**9856–9867.
28. **Miller, D. J., M. D. Schwartz, and P. Ahlquist.** 2001. Flock house virus RNA replicates on outer mitochondrial membranes in *Drosophila* cells. J. Virol. **75:**11664–11676.
29. **Miller, S., and J. Krijnse-Locker.** 2008. Modification of intracellular membrane structures for virus replication. Nat. Rev. Microbiol. **6:**363–374.
30. **Noueiry, A. O., and P. Ahlquist.** 2003. Brome mosaic virus RNA replication: revealing the role of the host in RNA virus replication. Annu. Rev. Phytopathol. **41:**77–98.
31. **Nugent, C. I., K. L. Johnson, P. Sarnow, and K. Kirkegaard.** 1999. Functional coupling between replication and packaging of poliovirus replicon RNA. J. Virol. **73:**427–435.
32. **Paliwal, Y. C.** 1970. Electron microscopy of Bromegrass mosaic virus in infected leaves. J. Ultrastruct. Res. **30:**491–502.
33. **Rao, A. L.** 2001. Bromoviruses, p. 155–158. *In* O. C. Maloy and T. D. Murray (ed.), Encyclopedia of plant pathology. John Wiley & Sons, Mississauga, Ontario, Canada.
34. **Rao, A. L.** 2006. Genome packaging by spherical plant RNA viruses. Annu. Rev. Phytopathol. **44:**61–87.
35. **Rao, A. L., and B. Cooper.** 2006. Capsid protein gene and the type of host plant differentially modulate cell-to-cell movement of cowpea chlorotic mottle virus. Virus Genes. **32:**219–227.
36. **Rao, A. L., and G. L. Grantham.** 1996. Molecular studies on bromovirus capsid protein. II. Functional analysis of the amino-terminal arginine-rich motif and its role in encapsidation, movement, and pathology. Virology **226:**294–305.
37. **Restrepo-Hartwig, M., and P. Ahlquist.** 1999. Brome mosaic virus RNA replication proteins 1a and 2a colocalize and 1a independently localizes on the yeast endoplasmic reticulum. J. Virol. **73:**10303–10309.
38. **Restrepo-Hartwig, M. A., and P. Ahlquist.** 1996. Brome mosaic virus helicase- and polymerase-like proteins colocalize on the endoplasmic reticulum at sites of viral RNA synthesis. J. Virol. **70:**8908–8916.
39. **Schaad, M. C., P. E. Jensen, and J. C. Carrington.** 1997. Formation of plant RNA virus replication complexes on membranes: role of an endoplasmic reticulum-targeted viral protein. EMBO J. **16:**4049–4059.
40. **Schlegel, A., T. H. Giddings, Jr., M. S. Ladinsky, and K. Kirkegaard.** 1996. Cellular origin and ultrastructure of membranes induced during poliovirus infection. J. Virol. **70:**6576–6588.
41. **Schonborn, J., et al.** 1991. Monoclonal antibodies to double-stranded RNA as probes of RNA structure in crude nucleic acid extracts. Nucleic Acids Res. **19:**2993–3000.
42. **Schwartz, M., et al.** 2002. A positive-strand RNA virus replication complex parallels form and function of retrovirus capsids. Mol. Cell **9:**505–514.
43. **Schwartz, M., J. Chen, W. M. Lee, M. Janda, and P. Ahlquist.** 2004. Alternate, virus-induced membrane rearrangements support positive-strand RNA virus genome replication. Proc. Natl. Acad. Sci. U. S. A. **101:**11263–11268.
44. **Snijder, E. J., et al.** 2006. Ultrastructure and origin of membrane vesicles associated with the severe acute respiratory syndrome coronavirus replication complex. J. Virol. **80:**5927–5940.
45. **Staehelin, L. A.** 1997. The plant ER: a dynamic organelle composed of a large number of discrete functional domains. Plant J. **11:**1151–1165.
46. **Tan, R., and A. D. Frankel.** 1995. Structural variety of arginine-rich RNA-binding peptides. Proc. Natl. Acad. Sci. U. S. A. **92:**5282–5286.
47. **Targett-Adams, P., S. Boulant, and J. McLauchlan.** 2008. Visualization of double-stranded RNA in cells supporting hepatitis C virus RNA replication. J. Virol. **82:**2182–2195.
48. **Venter, P. A., N. K. Krishna, and A. Schneemann.** 2005. Capsid protein synthesis from replicating RNA directs specific packaging of the genome of a multipartite, positive-strand RNA virus. J. Virol. **79:**6239–6248.
49. **Venter, P. A., D. Marshall, and A. Schneemann.** 2009. Dual roles for an arginine-rich motif in specific genome recognition and localization of viral coat protein to RNA replication sites in flock house virus-infected cells. J. Virol. **83:**2872–2882.
50. **Voeltz, G. K., M. M. Rolls, and T. A. Rapoport.** 2002. Structural organization of the endoplasmic reticulum. EMBO Rep. **3:**944–950.
51. **Weber, F., V. Wagner, S. B. Rasmussen, R. Hartmann, and S. R. Paludan.** 2006. Double-stranded RNA is produced by positive-strand RNA viruses and DNA viruses but not in detectable amounts by negative-strand RNA viruses. J. Virol. **80:**5059–5064.
52. **Wei, T., et al.** 2010. Sequential recruitment of the endoplasmic reticulum and chloroplasts for plant potyvirus replication. J. Virol. **84:**799–809.
53. **Wei, T., and A. Wang.** 2008. Biogenesis of cytoplasmic membranous vesicles for plant potyvirus replication occurs at endoplasmic reticulum exit sites in a COPI- and COPII-dependent manner. J. Virol. **82:**12252–12264.
54. **Welsch, S., et al.** 2009. Composition and three-dimensional architecture of the dengue virus replication and assembly sites. Cell Host Microbe **5:**365–375.
55. **Westaway, E. G., A. A. Khromykh, and J. M. Mackenzie.** 1999. Nascent flavivirus RNA colocalized in situ with double-stranded RNA in stable replication complexes. Virology **258:**108–117.
56. **Yamamoto, K., et al.** 2001. The KDEL receptor mediates a retrieval mechanism that contributes to quality control at the endoplasmic reticulum. EMBO J. **20:**3082–3091.
57. **Zlotnick, A., R. Aldrich, J. M. Johnson, P. Ceres, and M. J. Young.** 2000. Mechanism of capsid assembly for an icosahedral plant virus. Virology **277:** 450–456.